P8 Exploring new Architectures for Compressed Sensing Reconstructions in the MeerKAT era

Jonas Schwammberger

January 30, 2019

Abstract

The new MeerKAT Radio Interferometer poses an image reconstruction problem on a large scale. It measures an incomplete set of Fourier components, which have to be reconstructed by an imaging algorithm. Compressed Sensing reconstructions have the potential to improve the effective accuracy of MeerKAT, but so far have higher runtime costs compared to state-of-the-art CLEAN implementation. Both Compressed Sensing and CLEAN reconstructions use the non-uniform FFT approximation to cycle between Fourier and image space. But compared to CLEAN, Compressed Sensing algorithms need more cycles to converge, which is one of the reasons why they have higher runtime costs.

In this project, we investigate if Compressed Sensing algorithms can reduce the costs by replacing the non-uniform FFT approximation. We discuss three alternatives and create a new algorithm which does not need the non-uniform FFT during optimization. We leveraged the starlet transform and created a Compressed Sensing algorithm, which only needs to calculate the transform for non-zero basis functions. This allows us to use the direct Fourier Transform, which naturally extends to wide field of view measurements without any approximations. We demonstrate superior image quality on simulated data and extrapolate the runtime costs to a real-world MeerKAT observation. Compared to CLEAN, our algorithm was unable to reduce the runtime costs of large scale reconstructions.

Creating a scalable image reconstruction algorithm for MeerKAT is still an open problem.

In the large scale MeerKAT problems, calulating the Fourier Transform becomes an issue. Current Compressed Sensing implementations and CLEAN use the non-uniform FFT approximation, which leads to a similar architecture. In this work, we discuss three alternatives to the non-uniform FFT. We created a new algorithm which uses the direct Fourier Transform and Coordinate Descent. It does not need the approximation and naturally extends to wide field of view measurements of MeerKAT. Our algorithm leverages the starlet transform and only needs to calculate the transform for non-zero bases. This leads to a reconstruction algorithm, which scales with the number of non-zero components.

We compare our Coordinate Descent algorithm to CLEAN on simulated MeerKAT data. WE show the superior reconstruction quality and extrapolate the runtime costs of our approach to a real-world MeerKAT observation. Sadly, our algorithm could not improve the runtime costs compared to CLEAN. Coordinate Descent has interesting properties for distribution, but in the current state our algorithm is too expensive to be competitive.

We postulate that there is no single a

Contents

1 Compressed Sensing Image Reconstruction for MeerKAT

Image reconstruction problems arise in a variety of fields. From Medicine to Astronomy, imaging instruments are dealing with some level of corrupted measurements. Noise from the instrument itself, external interference or loss of samples, all introduce corruptions that a reconstruction algorithm should remove.

An algorithm should decide which part of the image is noise, and which is the image. It needs a prior for what an image is. This has led to the theory of Compressed Sensing[1, 2], which gives us a theoretical framework for analysis and design of reconstruction algorithms. It gives us theoretical guarantees that, under the right prior, an algorithm is guaranteed to reconstruct the observed image, potentially above the accuracy limit of the instrument.

In this work we apply the theory of Compressed Sensing to the reconstruction problem of Radio Interferometers. More specifically, we apply it on the MeerKAT interferometer, which poses the problem on a new scale of data volume. The raw measurement easily take up several hundreds of gigabytes, which should get reconstructed to an image. The current state of the art reconstruction is based on the CLEAN[3, 4] algorithm. Although newer Compressed Sensing reconstructions showed superior image quality[5, 6], they are more expensive to compute than CLEAN.

MeerKAT in the future will only produce more data. The reconstruction algorithm has to be scalable and sooner or later distributable. So far, state of the art CLEAN algorithm can distribute some steps, has limited capabilitiy of distribution. How to get a reconstruction algorithm to scale for future MeerKAT data is still an open problem.

In this project we investigated different reconstruction architectures for Compressed Sensing. Our task was to reduce the overall runtime costs compared to CLEAN. We created a Compressed Sensing reconstruction in a new architecture, which uses the direct Fourier Transform. It scales with the number of sparse components. We showed superior reconstruction quality than CLEAN. We extrapolate the runtime costs of our approach on MeerKAT scale reconstructions. Sadly, this architecture alone does not lead to runtime cost reduction compared to CLEAN or other state of the art approaches.

Nevertheless, it our algorithm might be easier to distribute. When combined with other concepts, we might arrive at a cheaper reconstruction algorithms.

We postulate that there is no single step which will get us to to the target of a highly scalable, highly distributable Compressed Sensing reconstruction. At the current point, there is no obvious way

We begin by introducing the basic image reconstruction problem in radio interferometry and show what the current architecture of interferometric reconstruction algorithms, the Major Cycle. Section 2 introduces the difficulties of imaging MeerKAT data. We move towards competing architectures in section 3. In the following sections 4, 5 and 6 we introduce our Compressed Sensing Reconstruction, show the reconstruction quality on simulated MeerKAT data and extrapolate the runtime costs on a real world MeerKAT measurement.

1.1 The basic reconstruction problem in Radio Interferometry

We start with a simplified measurement equation for Radio Interferometers, (1.1). An interferometer measures an incomplete set of Fourier Components V (called Visibilities in Radio Astronomy) from the sky image I at position x and y. We want to reconstruct the image $I()$, while the instrument measures $V()$ in a noisy environment. Since the term $e^{2\pi i(ux+vy)}$ is the Fourier Transform, the image can be calculated from the Visibilities by simply using the inverse Fourier Transform.

$$V(u,v) = \int\int I(x,y)e^{2\pi i(ux+vy)}\,dx\,dy \tag{1.1}$$

However, the Visibilities are incomplete and noisy. The inverse Fourier Transform does not give us the observed image, but a corrupted ”dirty” image. The incomplete Visibility coverage effectively convolves the observed image with a Point Spread Function. It introduces structures in the dirty image which were not observed. A reconstruction algorithm has to decide which structures were truly observed, and which are due to noise and incomplete Visibility coverage. In the framework of Compressed Sensing, this leads us to a minimization problem with the following objective function:

$$\underset{x}{minimize} \ \|V - Fx\|_2^2 + \lambda \|P(x)\|_1 \tag{1.2}$$

The objective (1.2) is split into two terms, the data and regularization term. The data term forces the reconstructed image to be as close to the measurements as possible, while the regularization term penalises unlikely images. Overall, we try to find the optimal image, which is as close to the Visibilities as possible, but also has the smallest regularization penalty according to some prior function $P()$. The parameter λ weights the trade-off between the data and regularization term. The theory of Compressed Sensing states that if our prior function $P()$ models the observed image well, it will be at the minimum of our objective function (1.2).

In theoretical terms, the reconstruction problem for Interferometers boils down to finding a good prior function $P()$ for Radio Astronomy images, and an efficient optimization algorithm to minimize (1.2). For large scale reconstructions, the Fourier Transform Matrix F becomes expensive to either compute or keep in memory. F has the size of $M * N$, where M is the number of Visibilities and N the number of pixels. In MeerKAT reconstructions, we have millions of pixels and several billions of Visibilities. The explicit matrix F is too large to be practical. We cannot use the Fast Fourier Transform, because the interferometer measures an incomplete and non-uniformly sampled set of Visibilities.

The large Fourier Transform matrix is common for Radio Interferometric image reconstructions. MeerKAT just poses the same problem on a new scale. We use the word architecture to differentiate between how we deal with F, and what prior function the reconstruction algorithm uses. How we deal with the large matrix gives us certain advantages and disadvantages which do not seem to be explored in the Radio Astronomy community. The common way of dealing with F is to use an approximation, which leads to the Major Cycle architecture.

1.2 The Major Cycle Architecture

The Major Cycle architecture was created with CLEAN in mind. It uses the non-uniform FFT approximation to cycle between Visibility and image space. First, we describe the Major Cycle and CLEAN in detail, and then describe how current Compressed Sensing reconstructions use the same architecture with minor modifications.

$$\underset{x}{minimize} \ \|I_{Dirty} - x \star PSF\|_2^2 + \lambda \|x\|_1 \quad , \quad I_{Dirty} = \hat{F}^{-1}V \tag{1.3}$$

A CLEAN image reconstruction for radio interferometers consists of two different steps: A non-uniform FFT, and a CLEAN deconvolution. The non-uniform FFT approximates the inverse Fourier Transform and calculates the dirty image. The CLEAN deconvolution uses the Point Spread Function and deconvolves the dirty image. In the framework of Compressed Sensing, CLEAN approximately minimizes the objective (1.3), where $\hat{F}$ is the non-uniform FFT approximation. Both, the non-uniform FFT and the CLEAN deconvolutions are approximations. To increase the overall accuracy of the reconstruction, CLEAN is used inside the Major Cycle architecture depicted in figure 1. In each Cycle, the residual Visibilities get transformed by the non-uniform FFT, CLEAN approximates the deconvolution, and the new residual image gets transformed back to Visibilities. Over several Major Cycles the error from the non-uniform FFT and from the CLEAN deconvolutions get minimized.

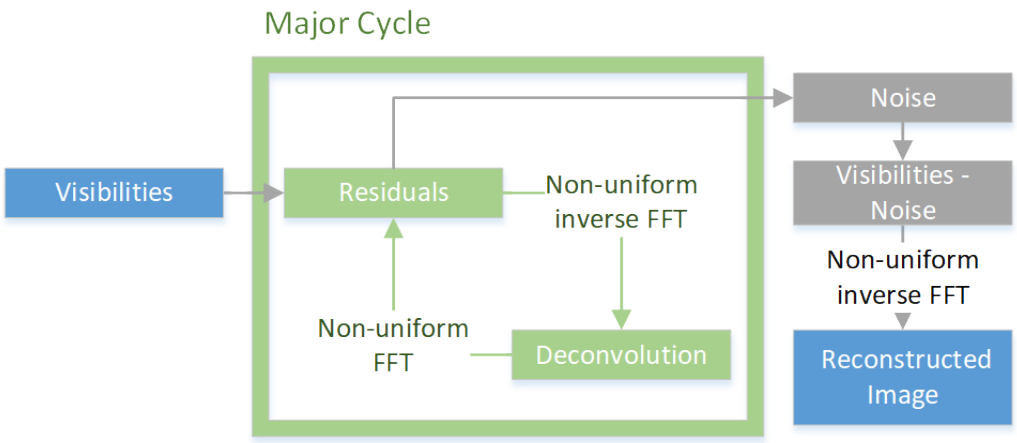

Figure 1: The Major Cycle Framework

The CLEAN objective (1.3) assumes that the observed image has few non-zero pixels, i.e. is sparse in the image domain. When the interferometer observed an image with only stars, which are concentrated on a single pixel, the observed image is at the minimum of the CLEAN objective.

Current Compressed Sensing reconstructions also use the non-uniform FFT and cycle between Visibility and image space[5, 6]. Although they do not use a deconvolution on the image, one can make the argument that they do not use the Major Cycle architecture. One of the main reasons why Compressed Sensing reconstructions are more expensive is because they need more non-uniform FFT cycles. Current research is focused on reducing the number of cycles[6]. However, since the non-uniform FFT is central to the Major Cycle, many approximations for realistic Interferometers made in section 2 can be used by the Compressed Sensing approaches. They are functionally similar. In this work, we group CLEAN and Compressed Sensing reconstructions with the non-uniform FFT together in the Major Cycle architecture.

2 Challenges for imaging MeerKAT data

We introduced the basic measurement equation and the imaging problem for Radio Interferometers. MeerKAT introduces a variety of new challenges for image reconstruction. In this work, we limit the scope to the third Fourier term of wide field of view imaging, and discuss the basics of calibration. Both directly affect how the reconstruction algorithm deals with the Fourier Transform and the wider architecture of the reconstruction. In this section, we look at the wide field of view measurement equation, discuss the basics of calibration and how they are solved in the Major Cycle architecture.

2.1 Wide Field of View Imaging and the third Fourier dimension

In wide field of view imaging, the simplifications we could make from the basic measurement equation (1.1) do not hold. The Visibility space of an interferometer actually has a third w-term. This leads us to the wide field of view measurement equation (2.1).

$$V(u,v,w) = \int\int \frac{I(x,y)}{\sqrt{1-x^2-y^2}} e^{2\pi i[ux+vy+w(\sqrt{1-x^2-y^2}-1)]}\, dx\, dy \tag{2.1}$$

For a small field of view, the term $\sqrt{1-x^2-y^2} \approx 1$, which simplifies to our original (1.1), we can ignore the w-term and use the two dimensional Fourier transform. Older interferometers typically created small field of view observations, where the basic measurement equation was accurate enough. But MeerKAT produces wide field of view observations. The w-term cannot be ignored anymore and has to be corrected. The figure 2b shows the effect of ignoring the w-term for wide-field of view observations. The image gets more distorted away from the center. Emissions at the edges of the image get ”torn” apart.

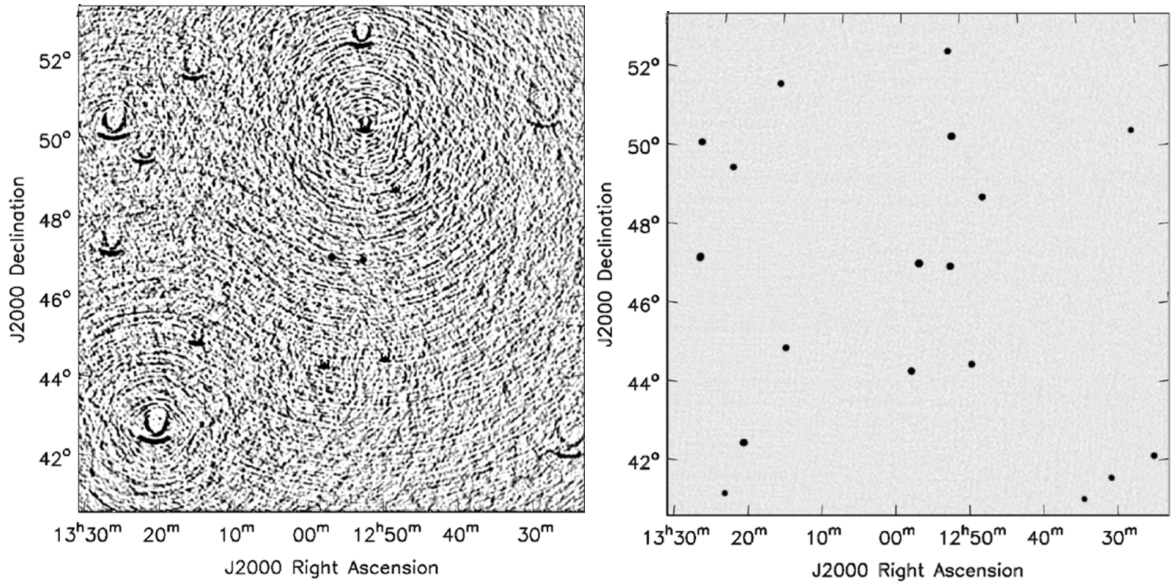

(a) 2D Fourier Transform. *(b) Fourier Transform with w-correction.*

Figure 2: Celestial sphere distortion on simulated data. Source: [7]

Let us look at the wide field of view measurement equation (2.1) in detail and explain this phenomenon. We see that the image $I(x,y)$ still two dimensional, even with a three dimensions in Visibility space. The observed image of the interferometer is not on a flat plane, but on a curved surface(hence the w-term)[8]. More precisely, the instrument looks at the inside wall of the celestial sphere. The two dimensional Fourier

transform approximates the curved surface with a flat plane, where the tangent point is typically the image center. The further away we move from the tangent point, the more distortion gets added by the curvature, represented by the term $\sqrt{1-x^2-y^2}$. The curve adds a phase shift the further away we move from the tangent point. If the reconstruction algorithm ignores the w-component for a wide field of view, the phase-shift gets severe enough to decorrelate the Visibilities, "tearing" apart the image structures of (2).

The effect of the w-term is one example of a Direction Dependent Effect (DDE). Wide field of view imaging introduces a number of DDE's, like distortions from the ionosphere and bleed over from different polarization. Correcting for the DDE in the Major Cycle architecture is under research[9], and is therefore out of scope for this project. We only correct for the w-term which directly influences the Fourier Transform and the architecture of reconstruction algorithms.

2.1.1 State of the art: w-stacking algorithm

The third Fourier breaks the two dimensional relationship between image and Visibilities, which keeps us from using the non-uniform FFT in the Major Cycle architecture. Before the w-stacking algorithm was developed, a wide field of view image was faceted into image patches where the w-term could be approximated with the small field of view measurement equation. w-stacking is the state-of-the-art way of approximating for the w-correction in an efficient manner. It calculates a w-corrected dirty image from three dimensional Visibilities.

The w-stacking algorithm, shown in figure 3 replaces the non-uniform FFT. It groups the Visibilities with similar w-term into the same layer. Multiple layers are then stacked and transformed independently with the non-uniform FFT. For each stack, the w-correction is performed for the center w-component. The last step is summing over all stacked images, giving us the final dirty image. From here on a standard CLEAN deconvolution, or a Compressed Sensing algorithm can search for the observed image.

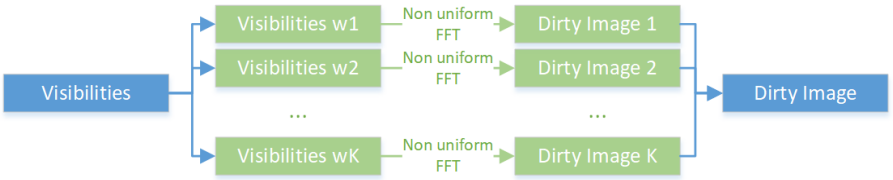

Figure 3: The Major Cycle Framework

Afterwards, the whole process is reversed. The image gets copied back into the stacks, the w-correction gets reversed and the non-uniform FFT calculates the Visibilities per stack.

If we choose uses as many stacks as Visibilities, we end up with an exact w-corrections. In practice, many Visibilities have a similar w-term. w-stacking approximates the correction and allows the Major Cycle to distribute the forward- and backwards non-uniform FFT to a certain extend.

2.2 Basic Calibration and Self-Calibration

The Visibilities measured by a Radio interferometer require calibration before an image can be reconstructed. Calibration corrects the amplitude and phase of the measured Visibilities for instrumental differences and direction independent effects. For small field of view instruments, this includes distortions from the ionosphere and other sources. The basic calibration scheme used a second observation where the true image was known, and solved for the missing calibration parameters C, shown in equation (2.2).

$$\underset{C}{minimize} \ \|CV_2 - F(x_2 \star PSF)\|_2^2 \tag{2.2}$$

V_2 are the Visibilities from the calibration observation, and x_2 is the known image. The resulting calibration parameters are then used in the observation of interest. The number of calibration parameters depends on the instrument and the observation, but is a fraction of the total number of Visibilities. Again, wide field of view tends to increase the number of necessary calibration parameters. Furthermore the true calibration drifts with time. Note that the equation (2.2) is essentially the reverse operation of image reconstruction. In this task, we want to find the calibration parameters from a known image.

This has led rise to the self-calibration scheme, were the observed image is solved for together with the calibration parameters C. We iteratively reconstruct the image with the current calibration, and then improve the calibration from the current image.

This has led to much better calibration and is very important for MeerKAT.

Self-Calibration pushes the calibration problem to the reconstruction algorithm.

3 Alternatives to the Major Cycle

Many Compressed Sensing reconstructions use the Major Cycle architecture[5, 6, 8, 10] and do not discuss alternatives. Pratley et al[11] optimized the non-uniform FFT in the context of Compressed Sensing reconstructions. Dabbech et al.[12] investigated w-term approximations for reducing runtime costs of Compressed Sensing reconstructions.

Although Compressed Sensing algorithms produce higher quality reconstructions, the CLEAN algorithm so far has lower runtime costs. Both use a version of the Major Cycle architecture for efficient transformation of Visibilities to image space, and to correct the effects of wide field of view imaging. This project explores three different ways of calculating the Fourier transform which leads to three different architectures. In this section we discuss the merits of each alternative in the context of reducing the cost for MeerKAT reconstructions.

3.1 Optimal projection on a uniform grid

In each iteration, the Major Cycle reduces the error from both, the non-uniform FFT approximation, and from incomplete measurements. Here, we discuss the potentials and problems of separating the problem into two optimization objectives (3.1) (3.2) and solve each after the other. This architecture first uses the optimal projection on a uniformly sampled grid, which is several times smaller than the original Visibility measurements.

$$\underset{I_{dirty}}{minimize} \left\| V - \tilde{F} I_{dirty} \right\|_2^2 \tag{3.1}$$

$$\underset{x}{minimize} \left\| I_{dirty} - x \star PSF \right\|_2^2 + \lambda \left\| P(x) \right\|_1 \tag{3.2}$$

The first objective (3.1) uses the non-uniform FFT approximation $\tilde{F}$ and searches for the optimal dirty image matching the Visibilities. The optimization algorithm for the first objective looks similar to the Major Cycle architecture. It still uses the non-uniform FFT approximation, and iteratively transforms the Visibilities to image space and back. In this architecture, we can use specialized optimization algorithms potentially uses fewer non-uniform FFT approximations to converge to the dirty image. At this point, we can drop the original Visibility measurements and only use the dirty image for further processing. The error introduced by the incomplete set of Visibilities can be represented as a convolution in image space with a Point Spread Function. The second objective (3.2) therefore can minimized to reconstruct the observed image x, which just needs the dirty image and the PSF.

The downside of this architecture lies in the PSF of the second objective. The PSF varies over the image. For the most accurate result, we would need a PSF for each pixel. The naive way to calculate a PSF for a pixel is to set all amplitudes of our Visibilities to 1, shift the phase to the desired pixel, and calculate the Fourier Transform. The naive way to calculate a PSF for each pixel leads to a quadratic runtime.

CLEAN gets away with a constant PSF[1], because of the Major Cycle architecture. In each cycle, it can reduce the error it introduced in the previous cycle, leading to a more accurate reconstruction. In the new architecture, we need several PSFs for a comparable accuracy to the Major Cycle, and this number dictates whether we can reduce the runtime costs. The question, how many PSFs are necessary, seems currently unknown in the Radio Astronomy community, as it becomes irrelevant for the Major Cycle. As of the time of writing, we do not know of any published research into this area. We do not have good estimates on the viability of this architecture.

[1] CLEAN implementations in Radio Astronomy typically use a constant PSF. This is not necessary, one can also implement CLEAN with a varying PSF.

The main advantage for this architecture is that it reduces the problem to a uniformly-sampled grid, and ignore the original Visibilities in later steps. However, in the context of self-calibration, we cannot ignore the non-uniformly sampled Visibilities. We need a transformation from the image back to the original Visibilities and improve the calibration parameters. Self-calibration negates the main advantage of the architecture. Unless we find a way to map the Visibilities together with their calibration parameters on a uniformly-sampled grid, this architecture does not seem practical for MeerKAT.

3.2 Spherical Harmonics

Spherical Harmonics are a different way to represent the measurements of an interferometer. Carozzi[14] derived a measurement equation based on the fact that the Visibilities fulfils the Helmholtz equation. In practical terms, Carozzi showed we can replace the non-uniform FFT with the Spherical Harmonics Transform in the Major Cycle architecture. Although the Spherical Harmonics Transform has interesting properties for full-sky imaging, this change alone neither leads to a different architecture, nor to a runtime improvement[2]

Compared to the Fourier domain, Spherical Harmonics naturally represent wide field of view interferometers and do not have a third dimension. This opens up new designs for Compressed Sensing reconstructions. For example, we can reconstruct the image by in-painting the missing Spherical Harmonics. Because they naturally represent curved surfaces, we can in-paint in a two dimensional space instead of three. Another direction is to image on the sphere directly. MCewen et al.[17] showed a way to put two dimensional wavelets on the sphere. A Compressed Sensing reconstruction can use a spherical wavelet as regularization and may simplify the transformation between measurements and reconstruction space.

Sadly, there is little published research in this area for Radio Astronomy image reconstructions. MCewen et al.[17] improved the runtime costs of simulations with the spherical Haar wavelet. Later work[8] showed a proof-of-concept Compressed Sensing reconstruction projected on the sphere, which improved the image quality. However, it did not use Spherical Harmonics and [8] is still based on the Fourier transform. At this point we have not found a proof-of-concept reconstruction algorithm which uses Spherical Harmonics to reduce runtime costs.

Although there seems untapped potential for new, cheaper reconstruction algorithms with Spherical Harmonics, practical limitations may explain the lack of research in this area. The Fourier relationship, Calibration, the effect of the ionosphere, everything discussed in section 2 is based on a plane wave arriving at the instrument[18, 19]. Spherical Harmonics are not. They are derived from a different property of the signal. The plane wave formalism may not translate to Spherical Harmonics. We may need to re-invent self-calibration, ionosphere distortion and more for Spherical Harmonic reconstructions.

3.3 Direct Fourier Transform

Hardy[13] replaced the non-uniform FFT with the direct Fourier Transform. It leads to a simplified architecture which naturally handles the w-term, but the whole Fourier matrix F has to be kept in memory. Using the direct Fourier Transform simplifies the architecture of the reconstruction. The drawback is either a large memory requirement for caching, or high runtime costs for continually calculating the transform matrix. For MeerKAT reconstructions where we reconstruct millions of pixels from several billions of Visibilities, the matrix becomes too large for any practical application.

However, the full Fourier matrix is not needed. Remember that CLEAN assumes the image is sparse, meaning only a few pixels are non-zero. In practice, even with extended emissions in the image, large regions of pixels are zero. They do not contribute to the reconstruction. Other Compressed Sensing reconstructions

[2] The fast Spherical Harmonics Transform is a generalization of the non-uniform FFT[15] and is still an active field of research[16].

showed that the reconstructed image can be more sparsely represented in an over-complete wavelet basis. Girard et al.[5] used the over-complete starlet transform, and Dabbech et al.[6] represent the image in several Daubechies frames. In a sparse reconstruction space, we only need to calculate the direct Fourier Transform for non-zero components of our basis, reducing the memory and runtime costs of the direct Fourier Transform.

In this project, we leverage the starlet transform and create an algorithm which uses the direct Fourier Transform for a few non-zero starlet components.

4 Compressed Sensing with Coordinate Descent and the direct Fourier Transform

Instead of using the Major Cycle architecture and approximate the non-uniform FFT approximation, we directly use the Fourier transform matrix F. We show the principle of our approach and of Compressed Sensing reconstructions in general at a simplified example. Let us minimize the objective function (4.1).

$$\underset{x}{minimize} \ \|V - Fx\|_2^2 + \lambda \|x\|_1 \tag{4.1}$$

The data term $\left\|V - F^{-1}x\right\|_2^2$ forces our image to be similar to the measurements, and the regularization term $\|x\|_1$ tells us how likely the current reconstruction is to be the true image. The parameter λ weights the trade-off between the data and the regularization term. With our term we assume our image contains only a limited number of non-zero pixels. When the instrument observes stars, they take up a single pixel in the image. In this case, our prior models the true image well, and the theory of compressed sensing states we are virtually guaranteed to find the truly observed image at the minimum of our objective function (4.1).

We can use a number of different optimization algorithms to optimize (4.1). Note however in the one dimensional case, where we only have one pixel, the data term of the objective (4.1) forms a parabola and the regularization term a shrink operation[3]. The optimum for a single pixel can be calculated by solving for the minimum of the parabola first, followed by a shrink operation. With Coordinate Descent we can exploit this property. We fix all pixels except for one and iteratively solve for the current minimum of each pixel. Now when we iterate over all pixels several times, we eventually converge to a solution. The full Coordinate Descent algorithm can be implemented in a few lines of python code:

```
def coordinate_descent(V_residual, x, lambda, max_iter):
  for k in range(0, max_iter):
    for i in pixels_row:
      for j in pixels_column:
        x_old = x[i, j]
        fourier_column = calculate_fourier_transform(i, j)
        fr = real(fourier_column)
        fi = imag(fourier_column)
        rr = real(V_residual)
        ri = imag(V_residual)

        #find apex
        a = sum(fr**2 + 2*fr*fi + fi**2)
        b = sum(fr*rr + fr*ri + fi*rr + fi*ri)
        x_new = b / a + x_old

        x_new = shrink(x_new, lambda)
        x[i, j] = x_new
        V_residual = V_residual - fourier_column * (x_new - x_old)
```

Coordinate Descent has to iterate over every pixels possibly several times. How quickly Coordinate Descent converges in theory is not well understood. Our optimization function (4.1) falls in the class of quadratic programming with a strictly convex objective. In this case, Coordinate Descent is guaranteed to converge at least linearly[20]. Sadly, real-world objective functions for image reconstruction are often not strictly convex. Usually our image is constrained to have only positive pixels[8], which breaks the strictly convex property of

[3] The shrink operation reduces the magnitude of the pixel by λ. For example: Pixel $x = -12.4$, $\lambda = 0.6$. The new pixel value after shrinkage follows as $shrink(-12.4, 0.6) = -11.9$

the objective function. In our environment, the convergence guarantees of Coordinate Descent are not well understood in theory.

In practice, Coordinate Descent can be improved with heuristics. Since we assume our image contains only a few stars, a few non-zero pixels, the simple Coordinate Descent algorithm wastes resources checking if the pixel is still zero. A better scheme would be the active set heuristic[21]: We iterate over every pixel once. Then, for a given number of iterations, we only check the pixels that have changed. This is an improvement, but too expensive in the context of MeerKAT. A reconstruction problem can have billions of Visibilities and serveral millions of pixels. Since F has the size of Visibilities times pixels, it gets too expensive to calculate all columns even once.

However, it turns out we do not need to if we imitate CLEAN: For CLEAN, the non-uniform FFT approximates the 'dirty' image, which is corrupted by the effects of incomplete measurements. CLEAN then subtracts a fraction of the PSF at the largest pixel value. In other words, the largest pixel value in the dirty image is the most likely non-zero pixel. We can use the dirty image approximation for a 'probability distribution' of non-zero pixels. It does not need to be accurate, since the actual reconstruction is done with the direct Fourier Transform.

This is, in principle, how the proof-of-concept algorithm works. Instead of reconstructing an image, it reconstructs in the starlet space. It uses the starlet transform of the dirty image to find likely non-zero components. Coordinate Descent is used to optimize single starlets. A proof-of-concept version of this algorithm was developed in python.

Although the algorithm produces super-resolved images in section 5, it is currently not known if it actually converges to the true optimum. Finding all relevant non-zero starlets is left to a greedy heuristic. There may be conditions under which it never includes relevant components. Further convergence analysis was outside the scope of the project. Also note that for this implementation, every time likely non-zero components are searched, it simply uses the non-uniform FFT for the dirty image approximation. This was done for simplicity's sake and can be improved.

4.1 The Starlet Transform

First we introduce the starlet transform, and then describe how we use it to estimate likely non-zero starlet components.

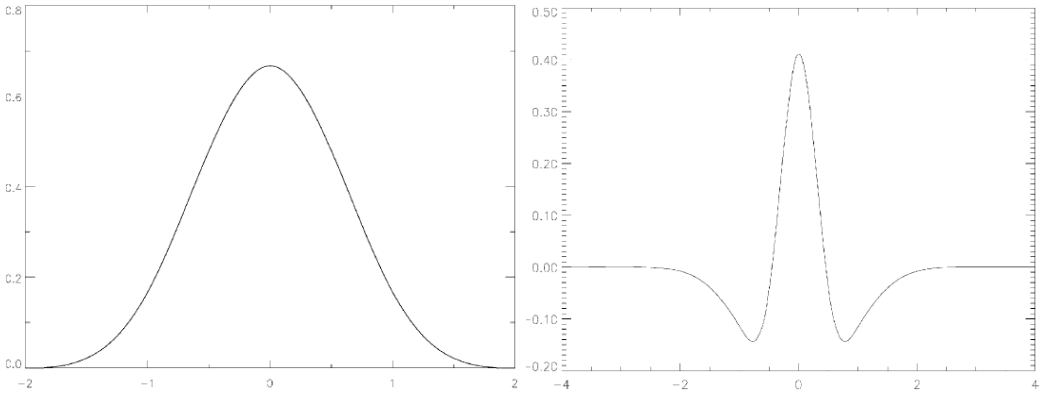

(a) Spline scaling function *(b) Wavelet function*

Figure 4: Scaling and wavelet function of the starlet wavelet. Source: [22]

The starlet transform is an Isotropic Undecimated Wavelet Transform (IUWT) with the starlet wavelet shown in figure 4. It defines two operations: The transformation from starlet into image space which is called synthesis,

and the inverse which is called decomposition. The starlet space represents an image in multiple layers at different scales, where lower layers contain smaller objects and upper layers the extended emissions. The lowest starlet layer represents the stars, while the upper layer represents the widest hydrogen clouds in the image.

$$\begin{aligned} c_0 &= \boldsymbol{x} \star B_0 \\ \boldsymbol{w_0} &= \boldsymbol{x} - c_0 \end{aligned} \tag{4.2}$$

Let us look at the lowest starlet layer first, how it is calculated from the image, and how we use it for image reconstruction. The starlet layer w_0 gets calculated in two steps, shown in (4.2). First, we take the scaling function for the lowest layer B_0, and convolve the image with it, resulting in the blurred image c_0. The blurring removes the smaller structures of the image. In the last step, we subtract the blurred image c_0 from x and arrive at the starlet layer 0, w_0. It contains the smallest structure of the image convolved with the starlet wavelet.

This is where the starlet transform ends. Note that we do not get the actual starlet components α_0 for the layer. The transformation just decomposes the structures of the image into layers. The actual starlet components α_0 would be the result of a deconvolution.

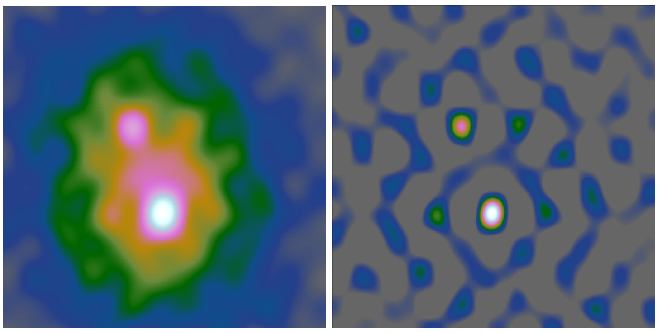

(a) Dirty Image with two point sources. *(b) Layer w_0 of the starlet decomposition.*

Figure 5: Dirty map and w_0 starlet layer after shrinkage. w_0 can be interpreted as a probability distribution for point source locations.

It turns out we can estimate the starlet components α_0 by simply shrinking the starlet layer w_0. Figure 5 shows an example of the process. Coordinate Descent will reconstruct the image with starlet components α_0, but it does not need to try all components. We use the starlet transform as a heuristic and can estimate likely non-zero α_0.

The same process is repeated for all J layers. We calculate the starlet decomposition shown in equation (4.3). We continually blur the image with ever wider scaling functions B_i. We subtract the more heavily blurred image c_{J-1} from c_{J-2} to arrive at the starlet layer, which contains the structures of the current size w_{J-1}. The scaling function B_i widens exponentially, and the top level starlet spans an area of $5 * 2^{J-1}$ pixels. Note that the last starlet layer is the most blurred version of the image c_J. It contains all structures which were wider than the widest starlet.

$$\begin{aligned} c_0 &= \boldsymbol{x} \star B_0 \\ \boldsymbol{w_0} &= \boldsymbol{x} - c_0 \end{aligned} \qquad \begin{aligned} c_1 &= c_0 \star B_1 \\ \boldsymbol{w_1} &= c_0 - c_1 \end{aligned} \qquad \dots \qquad \begin{aligned} c_{J-1} &= c_{J-2} \star B_{J-1} \\ \boldsymbol{w_{J-1}} &= c_{J-2} - c_{J-1} \end{aligned} \qquad \boldsymbol{c_J} = c_{J-1} \star B_J \tag{4.3}$$

We shrink all the starlet layers w_i and c_J, and arrive at which components α_i are likely non-zero. Coordinate Descent converges on the optimal α_i for all layers. At this point, we can reconstruct the image by reversing

the process. We convolve α_i with the starlet wavelet at scale i, which gives us w_i. Then, we sum them up to the final image (4.4).

$$\boldsymbol{x} = \boldsymbol{w_0} + \boldsymbol{w_1} + \ldots + \boldsymbol{w_{J-1}} + \boldsymbol{c_J} \tag{4.4}$$

This is how we leverage the starlet transform for our Coordinate Descent algorithm. Note that we can use the starlet transform as a heuristic without necessarily using the starlet components α_i for reconstructions. The starlet transform gives us likely locations of Gaussian-shaped emissions at different scales. We can for example use a Gaussian mixture model, and just use the starlets for likely non-zero locations.

In this work, we do not use the wavelet shown in image 4b. Instead, we modified the starlet to an extend where it arguably is not a wavelet any more. Still, the starlet transform with the correct wavelet as a heuristic, but reconstructed the image with a modified starlet to satisfy the non-negativity constraint.

4.1.1 Non-negative Starlet Modification

Reconstruction algorithms for Radio Astronomy typically constrain the image to be non-negative[8]. We can constrain the starlet components α_i to be non-negative, but the starlet wavelet has negative sections. Which leads to negative areas in the layers w_0, and negative pixel values in the reconstructed image x.

The simple fix is to either set all negative pixels of x to zero, or to set negative values of w_i to zero. Both lead to slightly different artefacts in the x, and both do not lead to significantly better results.

For reconstruction, we modify the starlet wavelet and set all negative sections to zero. At this point, the reconstruction starlet is arguably not a wavelet any more, since its integral is larger than zero. But now the Coordinate Descent algorithm can reconstruct a non-negative image which has led to a more sparse representation of images in the next section.

4.2 Proof of concept Implementation

In this section, we put together the starlet transform and the Coordinate Descent to form our algorithm. We use two separate loops of Coordinate Descent minimization. First, let us look at the objective function (4.5) for a single starlet layer and discuss why we still need the non-uniform FFT for pre-calculation.

Our target is to use as few columns from F as possible. As we have seen in equation (4.3), each starlet is a series of convolutions. We can also do the convolution in Fourier space, and we only need to calculate the columns of F for non-zero starlets instead of non-zero pixels. This leads us to the following objective (4.5) for a single layer i.

$$\underset{\alpha_i}{minimize}\ \|V - S_i F \alpha_i\|_2^2 + \lambda \|\alpha_i\|_1 \tag{4.5}$$

The drawback is that we need to calculate all the convolutions for the starlets at layer i in the non-uniformly sampled Fourier space. We used the non-uniform FFT approximation to calculate all S_i. This introduces an approximation again. In the future, one can find the optimal S_i in the non-uniform Fourier space by solving an optimization problem similar to objective (3.1). The starlet is constant for a given observation, which means we can pre-calculate all S_i before the optimization.

4.2.1 Iteration Scheme and Heuristics

Our algorithm is split in two separate Coordinate Descent loops. The first ”adding” loop, iterates over the starlet components of a single layer. Here we use the starlet transform as a heuristic and add likely non-zero components. The second, ”sparsifying” loop iterates over all non-zero components of all layers. Together they form one full iteration of our proof-of-concept algorithm.

```
def one_full_iteration(V_residual, alpha, J, lambda):
  #adding loop
  for j in reverse(range(0, J)):
    a = alpha[j]
    active_set = starlet_decomposition(non_uniform_fft(V_residual), lambda)
    a = coordinate_descent(V_residual, active_set, lambda, 10)

  #sparsifying loop
  non_zero = sum(abs(alpha))
  for i in range(0, 10):
    for j in range(0, J):
      a = alpha[j]
      active_set = a[non_zero > 0]
      a = coordinate_descent(V_residual, active_set, lambda, 1)
```

The adding loop minimizes the objective (4.5). We first use the starlet transform for estimating likely non-zero components. We then use Coordinate Descent and iterate over the likely non-zero components. In theory, the Coordinate Descent iterations in the adding loop are not necessary. The sparsifying loop will converge to the same solution. In practice, the Coordinate Descent iterations help to reduce the non-zero components we add. When we look again at image 5b, which shows the likely location of point sources, we see that the individual locations are not independent. Coordinate Descent iterations here help to reduce the number of non-zero starlets that get minimized in the sparsifying loop.

The adding loop minimized each layer separately. The task for the sparsifying loop is to minimize $alpha_i$ for all layers. In this implementation, we look at all α_i for each non-zero location in α. If the adding loop set a point source at a certain pixel location, the sparsifying loop checks if a wider starlet at the same location minimizes the objective.

Our modified starlet starlet

The starlet transform allows for a myriad of heuristics with Coordinate Descent. In the adding loop, we sort the active set heuristic.We leveraged another fact of the starlet transform

5 Test on simulated data

In this section, we test our new approach with Coordinate Descent on simulated MeerKAT data. We show that our approach does not need to calculate the whole Fourier Transform matrix F. Instead, we use a heuristic to only use relevant columns. As mentioned in section 4, it is unknown if our approach will converge to the true optimum. Nevertheless, we compare our results with CASA's CLEAN implementation, and demonstrate super-resolution performance of Coordinate descent together with accurate total flux modelling.

The two simulated datasets contains idealized MeerKAT observations. Compared to the real world, the two simulated datasets contain few Visibilities and not representative of the real data volume. Also, more realistic simulations which contain pointing-, calibration-, and thermal noise are out of scope for this project. The simulations are used to isolate the two fundamental issues in radio interferometer image reconstruction: Non-uniform sampling and incomplete measurements.

5.1 Super-resolution of two point sources

The first simulated observation contains two non-zero pixels, i.e. point sources, with intensity of 2.5 and 1.4 Jansky/Beam. The image has a size of 256^2 at a resolution of 0.5 arc-seconds per pixel. The integral, the total Flux of the image, is 3.9 Jansky/beam.

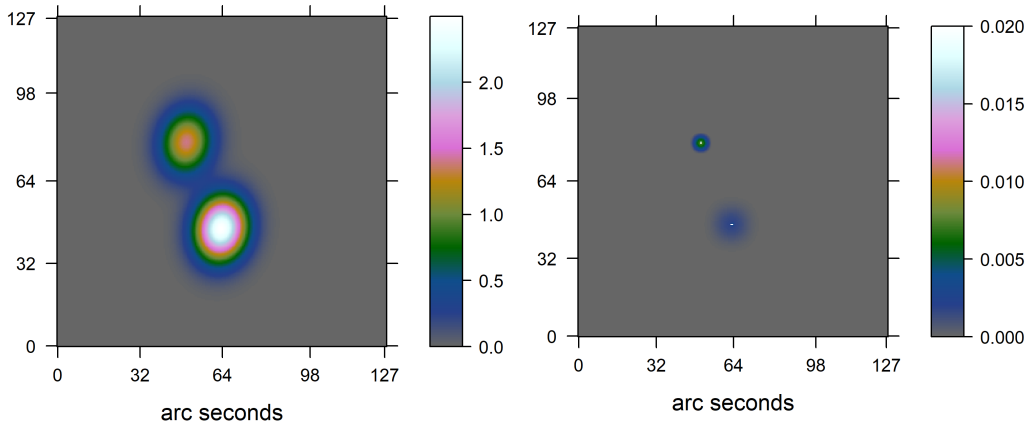

(a) CLEAN reconstruction with CASA standard parameters.

(b) Coordinate Descent reconstruction with $\lambda = 0.01, J = 4$.

Figure 6: Image reconstruction of two simulated point sources.

The figure 6 shows the CLEAN and the Coordinate Descent reconstruction. CLEAN reconstructs the image 6a at the accuracy limit of the instrument. It essentially reconstructs a blurred version of the observed image, where the blurring represents the accuracy of the instrument. With compressed sensing, we aim to reconstruct the de-blurred image, increasing the effective accuracy of the instrument.

Coordinate Descent in image 6b shows a super-resolved reconstruction of the two point sources. It reconstructs two narrow peaks surrounded,by a low-intensity Gaussian emission. Also, Coordinate Descent manages to capture the total flux more accurately than CLEAN. The total flux of image 6b results in 3.92 Jansky/beam, compared to CLEAN which overshoots the number by a factor of 1400. The total flux of the CLEAN reconstruction 6a overshoots the 3.9 figure by a factor of 1400. This gets obvious when we compare the intensity profile of CLEAN, Coordinate Descent and the ground truth in figure 7.

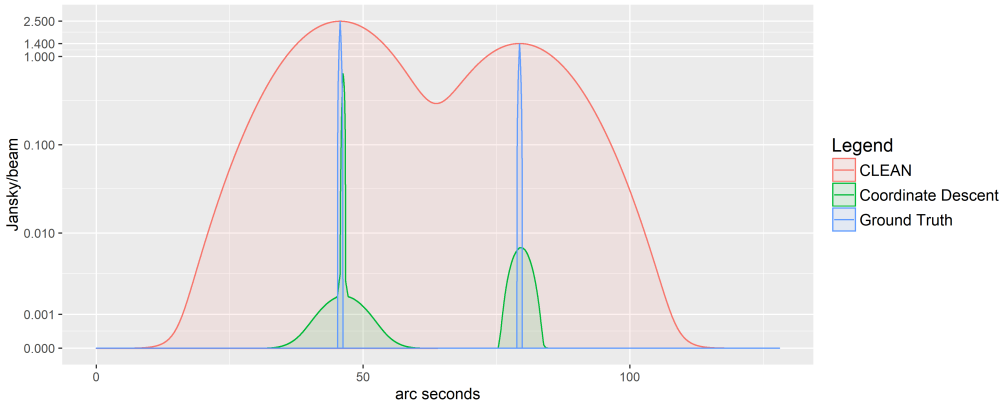

Figure 7: Intensity profile of the two point sources.

CLEAN essentially places a Gaussian function with correct peak intensity at the point source location, but it does not respect the total flux of the image. Coordinate Descent keeps the total flux in mind. The pixels in each area of the point sources sum up to the correct values of 2.5 and 1.4 respectively. However, note that Coordinate Descent in figure 7 seems to have both point sources shifted by approximately a pixel. It looks suspiciously like an off-by one error. Sadly in the time frame of this project, no error was found or an explanation for this behaviour.

5.2 Super resolution of mixed sources

This dataset contains a mixture of three Gaussian emissions and sixteen point sources of varying intensities. At the center of the image, it has three point sources underlying a weak extended emission. The image center and one Gaussian emissions are analysed in detail. Coordinate Descent was run for two full iterations, using $\lambda = 0.01$ and $J = 7$ starlet layers. The CLEAN and Coordinate Descent reconstructions are shown in figure 8. Our algorithm was able to locate the point sources below the accuracy limit of MeerKAT. However, some point sources were reconstructed with artefacts. We analyse two regions of the image in more detail.

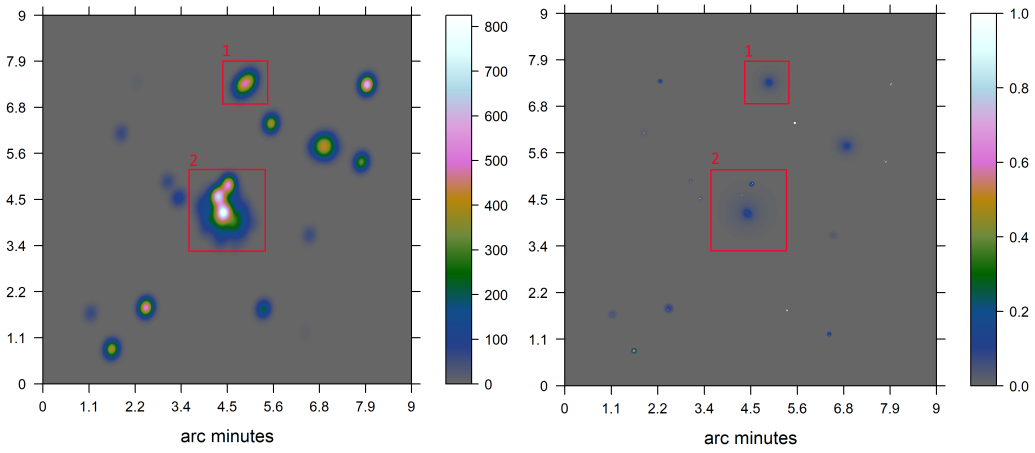

(a) CLEAN reconstruction *(b) Coordinate Descent Reconstruction*

Figure 8: Reconstruction on mixed sources

Let us look at the intensity profile of first region in figure 9. The Ground truth in image 9a shows a Gaussian extended emission with an oval shape. The figure 9b compares the intensity profile of Coordinate Descent

with CLEAN and the ground truth. The intensity profile on the logarithmic scale emphasises the artefacts of the starlet reconstructions. Coordinate Descent used three starlets at different scales to approximate the extended emission. It reconstructed the flux more accurately, but did not capture the shape of the extended emission. Instead, it approximated the oval shape with a uniform Gaussian-like emission. CLEAN on the other hand, did not again over-estimated the flux, but captured the oval shape more accurately.

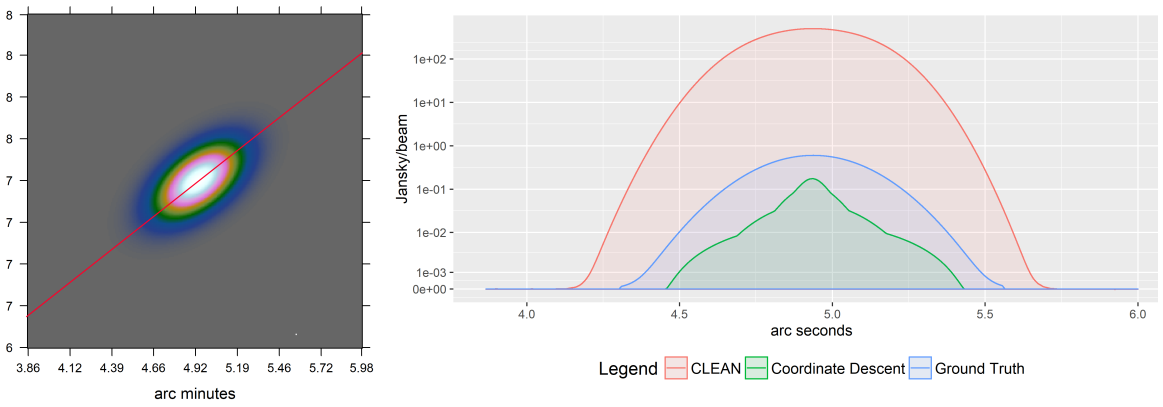

(a) Ground truth. *(b) Intensity profile.*

Figure 9: Intensity profile of region 1.

The second region in figure 10 is more complex. It contains an extended Gaussian emission with several point sources. The intensity profile is cut through the center and two point sources shown in the ground truth image 10a. CLEAN again accurately reconstructs the peak intensity of the point sources, but over-estimates the total flux of the region. Coordinate Descent separates the point source from the extended emission. Sadly, the first point source seems again shifted by a pixel, while the second point source was reconstructed with three peaks at varying intensities.

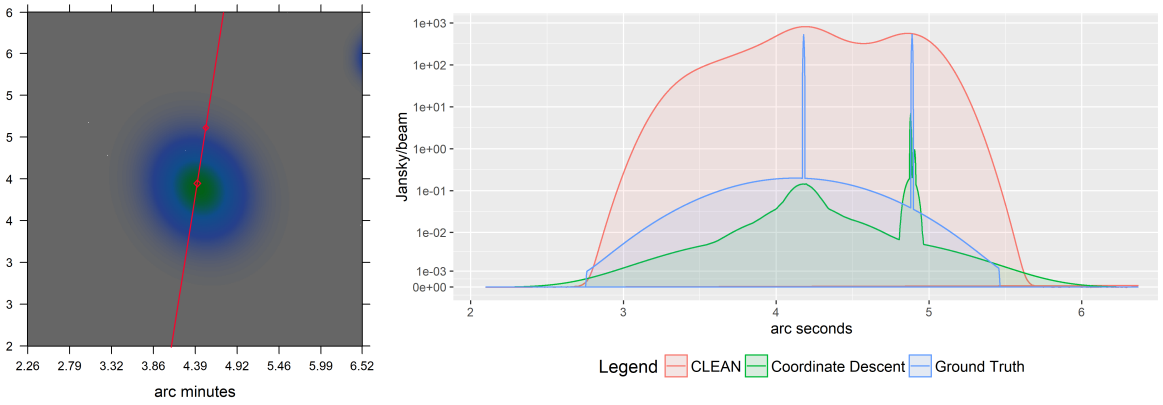

(a) ground truth *(b) ground truth*

Figure 10: Intensity profile of region 2.

Compared to CLEAN, Coordinate Descent with the modified starlet regularization reconstructed the image with a more accurate total flux, and located the point sources below the accuracy of the instrument. The quality of the point source reconstruction varies within the image 8b. The figure 11 shows four different point sources of in detail. From left to right, the reconstruction quality of each example decreases.

The left image shows shows a reconstruction where the flux is concentrated into a single pixel, and has low intensity emission around. Our modified starlet reconstruction should produce point sources similar to it. The second image from the left looks similar at first glance, but contains a lower intensity ”trail”. The third and

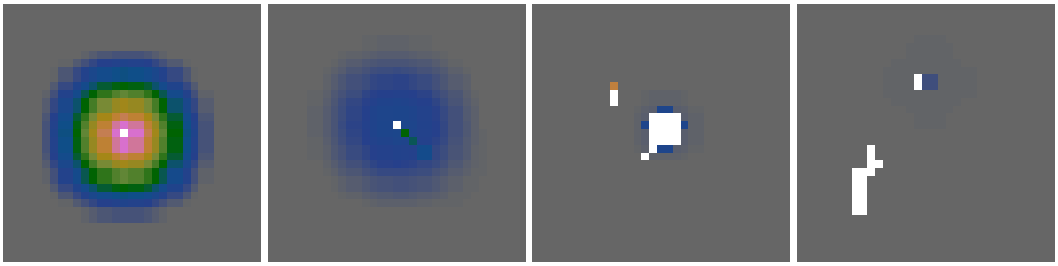

Figure 11: Different point source reconstructions of Coordinate Descent.

fourth image even contain a fake point source in close proximity.

Our modified starlet has likely a role in these artefacts. In section 4.1.1, we described how our modified starlet does not have negative sections. Intuitively, the original starlet penalizes two point sources in close proximity, and forces the emission to be represented with a wider starlet. Since we removed the negative sections, our algorithm can use as many point sources next to each other without any penalty. This would explain the ”trail” of single pixel emissions in the second, third and fourth images.

The original starlet wavelet forces the second, third and fourth image of figure 11 to be similar to the first, but at the cost of sparsity. Our modified starlet can represent the image 8b with 244 non-zero bases, while the original starlet leads to over 2000. It has to correct for the negative image regions it produces.

Our modified starlet leads to a more sparse solution, but may introduce artefacts in reconstructing point sources. In our proof-of-concept-implementation, we used the same λ regularization for each layer. Girard et al.[5] used a different λ for every layer. It may help reduce the artefacts of our modified starlet, while keeping the sparse representation it provides.

6 Runtime cost comparison on a real-world MeerKAT reconstruction

Current Compressed Sensing reconstructions produce images at a higher quality than CLEAN. However, CLEAN is significantly cheaper to compute. MeerKAT's large scale reconstruction problems, CLEAN is still the go-to algorithm. In this project, we developed for a new architecture, which uses the relevant columns of the Fourier Transform Matrix directly. We developed a Coordinate Descent algorithm with this architecture and demonstrated in section 5 super-resolution performance on simulated data. The question, if we can lower the runtime costs with our new architecture, is still open.

In this section, we compare the costs of Coordinate Descent with WSCLEAN, which is the reconstruction algorithm of choice for MeerKAT reconstructions. We create cost functions for each algorithm, which estimate the number of operations depending on the input size. WSCLEAN was executed on a real-world MeerKAT dataset shown in image 12. Our proof-of-concept implementation was not able to handle the large amount of data. Instead, we extrapolate the best-case costs of our approach and compare them to WSCLEAN on the MeerKAT dataset.

6.1 Cost function of an idealized Coordinate Descent

The runtime cost of Coordinate Descent depends on the number of Visibilities M and the number of non-zero starlets S. The number and location of the S non-zero starlets are generally not known. However, we created a heuristic which finds likely non-zero starlet components. In a realistic setting, the heuristic will have found more than S likely non-zero starlets. For the idealized version of Coordinate Descent, we assume an oracle performance heuristic: It finds the location and number of the S non-zero starlet components in constant time. Coordinate Descent therefore has to calculate the value of S components. In total, the idealized Coordinate Descent algorithm uses four steps: creating J starlet levels with the non-uniform FFT, creating the columns of F^{-1}, calculating the minima for each single component, and calculating the starlet layers:

$$\begin{aligned} J\text{non-uniform FFTs for the starlet regularization} &: J * (M + 2N * ld(2N)) \\ \text{creating } S \text{ columns of } F^{-1} &: S * 7M \\ \text{locating } S \text{ minima of } S \text{ parabolas} &: S * 4M \\ \text{calculating } J \text{ Starlet layers} &: J * 2M \end{aligned}$$

We assume we have enough memory to cache the columns of F^{-1} and only need to calculate them once. Keep in mind that each column of F^1 has the same length as the Visibilities, essentially multiplying the input data. The last parameter for Coordinate Descent is the number of iterations to converge, $I_C D$. Estimating this number is difficult as Coordinate Descent does not have strict guarantees (as discussed in section 4). Instead, we assume it converges after a fixed number of iterations. Therefore we arrive at the cost function of (6.1).

$$\begin{aligned} CD(I_{CD}, M, S, J) = & I_{CD} * [S * 4M + J * 2M] \\ & + S * 7M \\ & + J * (M + 2N * ld(2N)) \end{aligned} \tag{6.1}$$

Note that the runtime of Coordinate Descent is independent of the number of pixels. The only image related parameter in (6.1) is J, the number of starlet layers. The largest starlet layer represents the largest possible structure in the image, which is given by the instrument and the image resolution. The runtime only depends indirectly on the image resolution, not the total number of pixels. For simplicity, we assume the image cannot

have structures larger than half the image size. For our MeerKAT example, this is more than enough to represent the largest structures.

Also note the term iterating over the S non-zero starlets, $I_{CD} * [S * 4M + \ldots]$. As it turns out, this is the Achilles heel of the algorithm. MeerKAT observations contain a very large amount of Visibilities M.

6.2 Cost function of WSCLEAN

The WSCLEAN algorithm uses the Major Cycle architecture. It uses the non-uniform FFT with w-stacking. The runtime costs of a single Major Cycle depends on the non-uniform FFT with w-stacking and the number of CLEAN deconvolutions. N denotes the number of pixels.

$$\begin{aligned} \text{non-uniform FFT} &: M + 2N * ld(2N) \\ \text{non-uniform FFT with } w\text{-stacking} &: M + W * (2N * ld(2N) + 2N) + N * ld(N) \\ I_{CLEAN} \text{ deconvolutions} &: I_{WSCLEAN} * 2N \end{aligned}$$

The overall cost function shown in (6.2) can also be split into two parts. In each Major Cycle, the forward and backwards non-uniform FFTs gets calculated, and CLEAN deconvolves the image for a maximum number of I_{CLEAN} deconvolutions.

$$\begin{aligned} WSCLEAN(I_{Major}, I_{CLEAN}, M, N, W) = I_{Major} * 2 * [M + W * (2N * ld(2N) + 2N) + NlogN] \\ + [I_{CLEAN} * 2N] \end{aligned} \tag{6.2}$$

Notice that the number of CLEAN deconvolutions I_{CLEAN} depends on the image content, similar the number of non-zero starlets S for Coordinate Descent. Here however, it multiplies with the number of pixels instead of the number of Visibilities. In a sense, the major cycle tries to reduce the runtime complexity of handling the image content by calculating the non-uniform FFT. If the difference is large enough $N \ll M$, then the Major Cycle will end up with a smaller runtime costs.

6.3 Comparison on a MeerKAT reconstruction problem

Our real-world MeerKAT observation has been calibrated and averaged in frequency and time to reduce storage space. The resulting dataset contains 540 channels with 4 million Visibilities each. Due to hardware limitations, WSCLEAN was calculated on 75 channels. The reconstructed image is shown in 12, and the resulting parameters for our cost function are:

- Major Cycles: $I_{Major} = 6$
- Number of CLEAN iterations: $I_{CLEAN} = 35'000$
- Visibilities: $M = 3.05e^8$
- Pixels: $N = 2048^2$
- w-stacks: $W = 32$

For Coordinate Descent's costs, we need an estimate for J, S and I_{CD}. We set $J = 8$, which lets the largest structure span over half the image, enough to capture any large scale structures. For S and I_{CD}, we simply

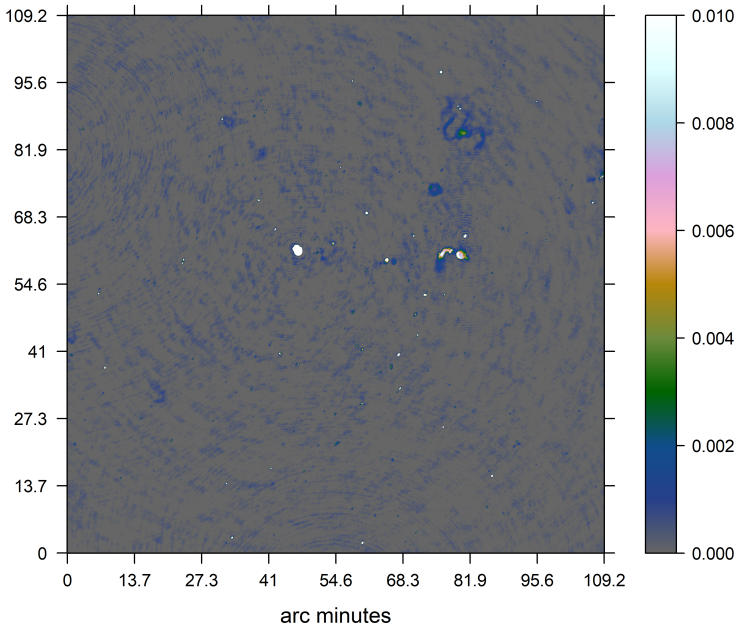

Figure 12: WSCLEAN Reconstruction of the MeerKAT observation.

use the values from our simulated reconstruction 8b and set $S = 250$ and $I_{CD} = 10$. This is an underestimation of the true values. The image 12 shows complex-shaped extended emissions, which likely needs a larger number of starlets for representation than the Gaussian emissions from our simulation.

When we put all values into our cost functions (6.1) and (6.2), Coordinate Descent with the direct Fourier transform arrives at 9.7 times the costs of WSCLEAN in the best case scenario. Our approach has not reduced the runtime costs compared to WSCLEAN. But what about Major Cycle Compressed Sensing algorithms? We have not developed a cost function for other Major Cycle approaches, but we can get a very rough estimate by changing I_{Major} of the WSCLEAN cost function. Pratley et al.[10] reported 10 Major Cycles for a Compressed Sensing reconstruction on simulated data. If we plug in 10 Major Cycles for WSCLEAN, Coordinate Descent ends up taking roughly 8 times the cost of the Major Cycle algorithm. Mind you these costs are only valid when we can keep all necessary columns of F in memory, eating up 1.1 terabytes[4] in our case. If not, the columns have to be re-calculated on the fly, increasing the runtime costs by magnitudes.

The issue with Coordinate Descent's runtime complexity lies in the term $I_{CD} * [S * 4M + \ldots]$ of (6.1), which scales with the "content" of the image S, multiplied with the Visibilities. Coordinate Descent cannot afford many iterations nor many non-zero components, because both of these numbers get multiplied together with M, the largest number in the problem. With the Major Cycle architecture, WSCLEAN is able to get around this limitation, and scales any content dependent factors on N instead of M.

Indeed, the runtime of our Coordinate Descent algorithm could be improved by using the Major Cycle architecture, essentially replacing M with N and we arrive at the term $I_{CD} * [S * 4N + \ldots]$. In this case Coordinate Descent can afford more iterations and more non-zero components for the same runtime costs. Furthermore N lies on a uniformly sampled grid. We may be able to use the FFT instead of caching columns of F, and reduce the memory requirement at the same time.

[4] If we assume 64 bit floating point accuracy for the real and complex values of the Visibilities.

6.4 Approximations as key for going large scale

We set out to reduce the runtime costs of compressed Sensing reconstructions by replacing the non-uniform FFT approximation. Ironically we ended up with an algorithm which not only has higher runtime costs, the costs may even be reduced by moving back to the Major Cycle architecture.

The question arises, whether the direct Fourier Transform has a future for MeerKAT reconstructions or not. From the current results we can summarize that the Major Cycle architecture with the non-uniform FFT is a good approximation of the Fourier Transform with no clear alternative. The emphasis is on the approximation. We do not need an exact transform. The Visibilities are inherently noisy, and even with the optimal reconstruction there will be residual noise in the image above the level of floating point accuracies. An optimal Fourier Transform for MeerKAT takes the inherent inaccuracy into account.

The direct Fourier Transform, as it is implemented in our algorithm, wastes resources with a precise transformation. In the context of MeerKAT, it has to re-introduce approximations to be competitive. Our Coordinate Descent approach leveraged the fact that not all columns of F are necessary for reconstruction. The next step is to see if the number of rows can be reduced too.

A MeerKAT reconstruction has magnitudes fewer pixels than Visibilities. Not all samples contribute the same amount of information to a reconstruction.If we can remove the redundant information before reconstruction, we can reduce the overall costs and increase the ratio of samples per pixel. Our Coordinate Descent algorithm scales independently of image size, the fewer samples we have per pixel, the more cost effective our algorithm becomes compared to CLEAN.

As it is, our proof-of-concept algorithm with the direct Fourier Transform is too expensive when compared to CLEAN. It wastes resources on a too precise transformation. By re-introducing approximations, we can further decrease the runtime costs of the direct Fourier Transform. Whether we can find an approximation, which is at least as accurate as the non-uniform FFT and has lower runtime costs remains to be investigated in the future.

7 Compressed Sensing reconstructions in the MeerKAT era

Current Compressed Sensing reconstructions share the non-uniform FFT approximation with CLEAN. Both continually cycle between Visibility an image space. Compared to CLEAN, Compressed Sensing algorithms need more cycles to converge, which is one of the reasons why they have higher runtime costs. In this project, we postulated that one may reduce the runtime cost of Compressed Sensing reconstructions by replacing the non-uniform FFT approximation.

We discussed three alternatives: Optimal Projection on a uniform Grid, using Spherical Harmonics and the direct Fourier Transform. With the latter approach, we created a proof-of-concept image reconstruction using Coordinate Descent. We leveraged the starlet transform and created an algorithm which scales with the number of non-zero basis functions. We demonstrated super-resolution performance on simulated MeerKAT data and extrapolated the runtime costs on a real-world observation. Compared to CLEAN and the non-uniform FFT, our algorithm leads to higher runtime costs. As it is implemented in this project, the direct Fourier Transform is not a viable alternative on MeerKAT data. The other two alternatives both have drawbacks which need to be resolved before they become viable.

Projecting on a uniform grid is way of potentially reducing the problem to a more manageable size. In this architecture, the first step is to use the optimal projection on a uniform grid. Later processing steps like reconstruction can be done on the uniform grid. However, self-calibration requires a transformation from uniform sampled grid back to the original measurements. In this task, we cannot ignore the original Visibilities in later processing. Unless one finds a way to project the calibration problem on a uniform grid too, self-calibration destroys the main advantage of the approach.

Spherical Harmonics are a new way to represent the Radio Interferometric Measurement Equation. We analysed published research in this area[14, 17] and see potential for a new reconstruction architecture, which may reduce the overall runtime costs. However, the current formalism[19] is based on the plane wave. How a real-world imaging algorithm with spherical harmonics deals with calibration and ionosphere distortion may be fundamentally different to current CLEAN and Compressed Sensing reconstructions. At this point, it is unclear if or how many imaging problems have to be re-investigated by moving to Spherical Harmonics.

There is no clear alternative to the non-uniform FFT approximation. It seems runtime efficient compared to the alternatives. MeerKAT only increases its data volume. Future imaging algorithms have to move to distributed computing eventually. State-of-the-art CLEAN can distribute some steps of the reconstruction. But not completely, and limited. Research is focussed on getting the non-uniform FFT, CLEAN and Compressed Sensing approaches to distribute. It is an inherently iterative reconstruction algorithm.

Here, the direct Fourier Transform can become interesting. It does not need an iterative approximation scheme, and may prove to be useful for distributed computing. If we can get the runtime costs to be more competitive.

Bayesian statistics.

Still an open question, we do not have any break-through

References

[1] Emmanuel J Candès, Justin Romberg, and Terence Tao. Robust uncertainty principles: Exact signal reconstruction from highly incomplete frequency information. IEEE Transactions on information theory, 52(2):489–509, 2006.

[2] David L Donoho. Compressed sensing. IEEE Transactions on information theory, 52(4):1289–1306, 2006.

[3] JW Rich, WJG De Blok, TJ Cornwell, Elias Brinks, Fabian Walter, Ioannis Bagetakos, and RC Kennicutt Jr. Multi-scale clean: A comparison of its performance against classical clean on galaxies using things. The Astronomical Journal, 136(6):2897, 2008.

[4] Urvashi Rau and Tim J Cornwell. A multi-scale multi-frequency deconvolution algorithm for synthesis imaging in radio interferometry. Astronomy & Astrophysics, 532:A71, 2011.

[5] Julien N Girard, Hugh Garsden, Jean Luc Starck, Stéphane Corbel, Arnaud Woiselle, Cyril Tasse, John P McKean, and Jérôme Bobin. Sparse representations and convex optimization as tools for lofar radio interferometric imaging. Journal of Instrumentation, 10(08):C08013, 2015.

[6] Arwa Dabbech, Alexandru Onose, Abdullah Abdulaziz, Richard A Perley, Oleg M Smirnov, and Yves Wiaux. Cygnus a super-resolved via convex optimization from vla data. Monthly Notices of the Royal Astronomical Society, 476(3):2853–2866, 2018.

[7] Tim J Cornwell, Kumar Golap, and Sanjay Bhatnagar. The noncoplanar baselines effect in radio interferometry: The w-projection algorithm. IEEE Journal of Selected Topics in Signal Processing, 2(5):647–657, 2008.

[8] Jason D McEwen and Yves Wiaux. Compressed sensing for wide-field radio interferometric imaging. Monthly Notices of the Royal Astronomical Society, 413(2):1318–1332, 2011.

[9] HT Intema, S Van der Tol, WD Cotton, AS Cohen, IM Van Bemmel, and HJA Röttgering. Ionospheric calibration of low frequency radio interferometric observations using the peeling scheme-i. method description and first results. Astronomy & Astrophysics, 501(3):1185–1205, 2009.

[10] Luke Pratley, Melanie Johnston-Hollitt, and Jason D McEwen. A fast and exact w-stacking and w-projection hybrid algorithm for wide-field interferometric imaging. arXiv preprint arXiv:1807.09239, 2018.

[11] Luke Pratley, Jason D McEwen, Mayeul d'Avezac, Rafael E Carrillo, Alexandru Onose, and Yves Wiaux. Robust sparse image reconstruction of radio interferometric observations with purify. Monthly Notices of the Royal Astronomical Society, 473(1):1038–1058, 2017.

[12] Arwa Dabbech, Laura Wolz, Luke Pratley, Jason D McEwen, and Yves Wiaux. The w-effect in interferometric imaging: from a fast sparse measurement operator to superresolution. Monthly Notices of the Royal Astronomical Society, 471(4):4300–4313, 2017.

[13] Stephen J Hardy. Direct deconvolution of radio synthesis images using l1 minimisation. Astronomy & Astrophysics, 557:A134, 2013.

[14] TD Carozzi. Imaging on a sphere with interferometers: the spherical wave harmonic transform. Monthly Notices of the Royal Astronomical Society: Letters, 451(1):L6–L10, 2015.

[15] Stefan Kunis, J Keiner, and D Potts. Nonequispaced fft. Available: www-user. tu-chemnitz. de/skunis/paper/lecturenfft. pdf.

[16] Nathanaël Schaeffer. Efficient spherical harmonic transforms aimed at pseudospectral numerical simulations. Geochemistry, Geophysics, Geosystems, 14(3):751–758, 2013.

[17] JD McEwen and AMM Scaife. Simulating full-sky interferometric observations. Monthly Notices of the Royal Astronomical Society, 389(3):1163–1178, 2008.

[18] Anthony Richard Thompson, James M Moran, George Warner Swenson, et al. Interferometry and synthesis in radio astronomy. Springer, 1986.

[19] Oleg M Smirnov. Revisiting the radio interferometer measurement equation-i. a full-sky jones formalism. Astronomy & Astrophysics, 527:A106, 2011.

[20] Zhi-Quan Luo and Paul Tseng. On the convergence of the coordinate descent method for convex differentiable minimization. Journal of Optimization Theory and Applications, 72(1):7–35, 1992.

[21] Jerome Friedman, Trevor Hastie, and Rob Tibshirani. Regularization paths for generalized linear models via coordinate descent. Journal of statistical software, 33(1):1, 2010.

[22] Jean-Luc Starck, Fionn Murtagh, and Mario Bertero. Starlet transform in astronomical data processing. Handbook of Mathematical Methods in Imaging, pages 2053–2098, 2015.

List of Figures

List of Tables

8 Ehrlichkeitserklärung

Hiermit erkläre ich, dass ich die vorliegende schriftliche Arbeit selbstständig und nur unter Zuhilfenahme der in den Verzeichnissen oder in den Anmerkungen genannten Quellen angefertigt habe. Ich versichere zudem, diese Arbeit nicht bereits anderweitig als Leistungsnachweis verwendet zu haben. Eine Überprüfung der Arbeit auf Plagiate unter Einsatz entsprechender Software darf vorgenommen werden.
Windisch, January 30, 2019

Jonas Schwammberger